PHOTOMASK

BACUS—The international technical group of SPIE dedicated to the advancement of photomask technology.

First Place Best Oral Paper PM11 8166-20

Evaluation of the Accuracy of Complex Illuminator Designs

Michael S. Hibbs, IBM Systems and Technology Group, Essex Junction, VT 05452

Jaione Tirapu-Azpiroz, IBM Microelectronics, Hopewell Junction, VT 12533

Kazunori Seki, Shinpei Kondo, Toppan Photomasks, Inc., Semiconductor Related Research Laboratory, Essex Junction, VT 05452

Gregory McIntyre, IBM Systems and Technology Group, Albany, NY 12203

ABSTRACT

Complex illuminators used for optical lithography or lithographic simulators typically have a slight loss of fidelity when compared to the original illuminator design. It is usually not obvious what the lithographic effects of this loss of fidelity will be. A series of computer-designed illuminators with multiple intensity levels was designed and built for use in an Aerial Image Measurement System[1,2] (AIMS™)+. Images of the various illuminators were recorded and correlated with the original designs. Images of photomasks with programmed defects were captured using these illuminators and the results were compared with simulations using the physical illumination pattern and the ideal illumination design. The results showed that small deviations between the illuminator design and the physically constructed illuminator had very little effect on the aerial images or defect sensitivity. Larger deviations from the illuminator design have increasingly significant effects on defect sensitivity.

1. Introduction

Off-axis illumination is a commonly used resolution enhancement method in optical lithography. The design of illuminators has become increasingly complex, progressing from simple circular illumination to annular, multipole, and finally computer-optimized pixellated illumination sources. These complex illuminator designs are physically generated using a variety of different devices, such as simple stencil apertures, diffractive optical elements, programmable micromirror arrays, or patterned filters fabricated from partially transparent light absorbers. Differences between the physically realized illumination and the original illuminator design might be expected to affect the accuracy of the aerial image projected by the optical system using the illuminator. In this paper we report on a series of measurements

Continues on page 3.

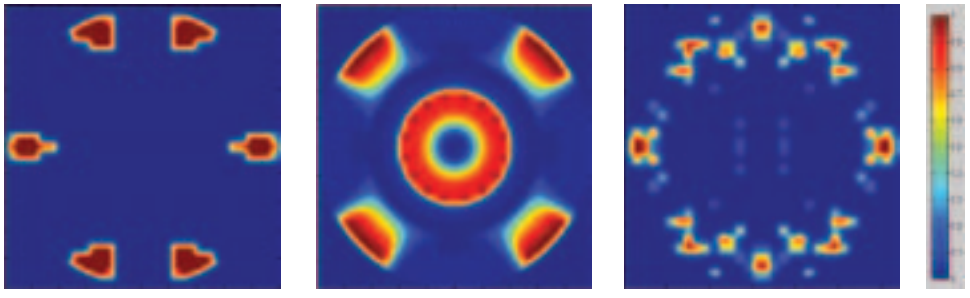

Figure 1. Designs for a binary stencil illuminator design (left), an emulated DOE design (center), and an SMO illuminator (right).

BACUS NEWS

DECEMBER 2011
VOLUME 27, ISSUE 12

TAKE A LOOK INSIDE:

SPIE

EDITORIAL

Industry Review

Michael D. Archuletta, RAVE LLC

As we come to the close of 2011, I thought I'd give you an overview of the status and forecast for the Photomask, Semiconductor and Electronics industries as well as the global macro economic conditions that directly influence these businesses.

To say the least, it's been an interesting few years. The global economic slow-down in 2008 (1.3% WGDP growth) and the worldwide recession in 2009 (-1.6% WGDP growth) conspired to produce two successive years of negative growth in the worldwide electronics industry (2008: -12%; 2009: -10%). The worldwide semiconductor industry is highly influenced by these factors and their global decline only served to worsen and prolong the deepest recession in semiconductor history (2008: -6%; 2009: -9%).

However, the semiconductor industry made a dramatic come-back in 2010. Year-To-Year (YTY) 2010 growth over 2009 was 30%+ (Table 1). The recovery of revenue spurred a 2010 YTY growth in semiconductor capital spending of more than 118%+. This resurgence in sales and capital spending created a bullish overall industry optimism going into 2011. In the spring of 2011, most researchers were forecasting 2011 semiconductor industry growth at 10%+.

Unfortunately, world events played a large part in mitigating this prediction. Unrest in the middle-east caused oil prices to surge. The devastating earthquake and tsunami in Japan severely disrupted supply chains in the electronics and semiconductor industries. Natural disasters in the United States burdened local economies affecting the U.S. GDP. The European debt crisis and the ongoing U.S. debt problems continue to create high levels of global economic uncertainty.

Semiconductor sales began to weaken in Q3-2011 generating overcapacity and rising inventory levels. All forecasters began lowering their 2011 semiconductor industry sales expectations to growth of 5% or less claiming the industry may again be facing a recession going into 2012. However, there are recent signs that inventory levels are diminishing and some companies are beginning to report increasing sales again. Industry analysts are seeing signs that this is a moderate down-turn cycle that will bottom-out and correct itself in the second quarter of 2012. Barring any future events that severely effect global GDP growth, predictions now run from 5% to as much as 10% YTY sales growth for the overall semiconductor sector.

	2010	2011F	2012F
World GDP*	$56.8T	$58.7T	$60.9T
Growth % YTY	*3.8%*	*3.3%*	*3.7%*
United States GDP*	$13.7T	$13.9T	$14.3T
Growth % YTY	*0.7%*	*1.7%*	*2.8%*
World Electronics Sales**	$1.2T	$1.3T	$1.4T
Growth % YTY	*10.8%*	*6.3%*	*7.2%*
Semiconductor Industry Sales***	$284.8B	$299.0B	$312.8B
Growth % YTY	*30.8%*	*5.0%*	*4.6%*
Semiconductor Capital Spending***	$56.5B	$61.8B	$51.5B
Growth % YTY	*118.4%*	*9.4%*	*-16.7%*
Photomask Industry Sales****	$3.0B	$3.2B	$3.3B
Growth % YTY	*10.0%*	*7.0%*	*2.0%*

Sources: *World Bank (September 2011); **IC Insights (September 2011); ***Gartner (September 2011); ****SEMI (April 2011

Figure 1.

(continues on page 7)

BACUS

N • E • W • S

BACUS News is published monthly by SPIE for BACUS, the international technical group of SPIE dedicated to the advancement of photomask technology.

Managing Editor/Graphics Linda DeLano
Advertising Teresa Roles-Meier
BACUS Technical Group Manager Pat Wight

SPIE

P.O. Box 10, Bellingham, WA 98227-0010 USA
Tel: +1 360 676 3290
Fax: +1 360 647 1445
SPIE.org
help@spie.org

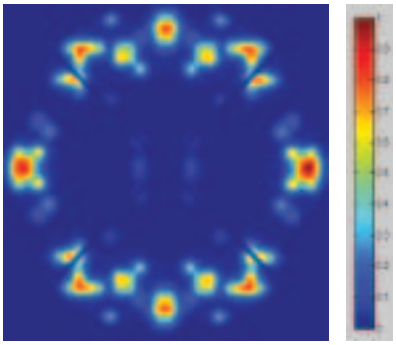

Figure 2. AIMS™ pupil image for the third design shown in figure 1 above.

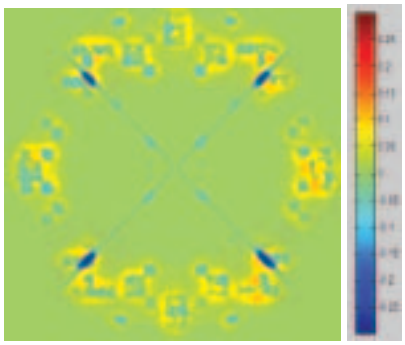

Figure 3. Difference plot between measured and designed illuminator.

to quantify the accuracy of illuminators used in an AIMS™ aerial image analysis tool.

2. Quantitative Measurement of Illuminator Accuracy

2.1 Illuminator design and construction

Several different illuminators were built to support mask manufacturing at the 65 nm through 20 nm lithographic nodes.

The illuminators tested were of three basic types: Complex stencil designs with binary intensity levels, emulations of Diffractive Optical Element (DOE) illuminators using graduated intensity levels, and Source Mask Optimization3,4 (SMO) designs with multiple pixellated gray-scale illumination spots. These illuminators were built using a patterning method that supports a continuous gradation of transmission levels in the design.

Figure 1 shows an example of each type of design.

Conventional illuminator designs (e.g. circular, annular, quasar, etc.) were also available, but were not evaluated in this study.

2.2 Image capture

The AIMS™ system has the capability to view and record the pupil illumination profile while exchanging and centering illumination apertures. An auxiliary lens called a Bertrand lens is moved into the optical path and focuses the pupil image onto a camera, which stores the image. The stored image does not have a normalized image intensity and the size of the minimum addressable picture element (pixel) is not the same as that of the source data used to specify the illuminator design. Still, it is easy to compare the physical illumination capture with the source data by appropriately adjusting the magnification scale, intensity scale, and X and Y offsets in a computer program.

The internal capture of the pupil image has both advantages and disadvantages compared to performing a transmission measurement of the illumination aperture on an optical bench. Because the pupil image is captured with the illuminator in its normal, aligned operating position, any non-uniformity in the laser illumination, darkened regions of the projection lens, or dirt spots in the optical system can be measured along with the illumination aperture's transmission. On the other hand, any imperfections in the Bertrand lens will be added to the illumination measurement, even though the Bertrand lens will be withdrawn from the optical path during actual use of the AIMS™ and will not actually contribute anything to the final AIMS™ image.

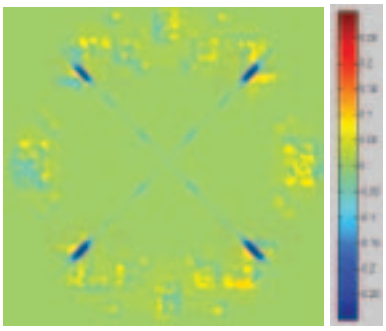

Figure 4. Improved match between measured pupil image and design after application of a Gaussian blurring function with σ=1.1 pixels.

2.3 Sample illuminator analysis

As an example of the analysis, figure 2 shows the AIMS™ image of the rightmost illuminator design in figure 1.

The recorded image and the original design have some differences. The low-intensity rows of spots near the center seemless clearly defined than in the design, and two diagonal dark lines can be seen in the image. The dark lines are gaps between segments of a 4-quadrant polarizer in the optical path. Illuminator designs should normally not have bright spots in these transitions between two regions of different polarization. The reduced contrast in the central spots could be caused by image flare or defocus from the Bertrand lens, or it could be a real loss of contrast from the manufacture of the illuminator.

Figure 3 shows the pupil illumination from figure 2 with the illuminator design subtracted. The background shade shows an exact match between measured illumination and the design, contrasting shades show the measured intensity higher or lower than design. The measured and design images were aligned and scaled to minimize the root-mean-square (RMS) deviation from zero in the difference plot.

The quality of the data matching is relatively good, with an RMS error of 3.4%, and a correlation of 0.9794 between the

Table 1. Quality of match to design for 14 different illuminator types. The second and third columns show RMS error and correlation coefficient for the pupil illumination as captured by the AIMS™. The fifth and sixth columns show the improvement in the match to design by convolving a Gaussian blurring function with the design data. The 1σ radius of the Gaussian is shown in column four.

Mask type and identification	RMS error of fit	Correlation coefficient	1σ radius of Gaussian blur (fraction of pupil radius)	RMS error of fit including Gaussian blur	Correlation coefficient including Gaussian blur
Stencil #1	2.02%	0.9958	0.016	1.31%	0.9980
Stencil #2	1.81%	0.9967	0.015	1.07%	0.9987
Stencil #3	2.03%	0.9952	0.015	1.04%	0.9986
DOE #1	3.04%	0.9963	0.019	2.20%	0.9978
DOE #2	1.82%	0.9984	0.024	1.64%	0.9985
DOE #3	2.10%	0.9979	0.018	1.55%	0.9987
SMO #1	2.40%	0.9922	0.016	1.12%	0.9980
SMO #2	2.41%	0.9915	0.016	1.20%	0.9975
SMO #3	2.85%	0.9905	0.018	1.84%	0.9954
SMO #4	3.06%	0.9864	0.017	2.17%	0.9924
SMO #5	3.42%	0.9794	0.018	2.66%	0.9853
SMO #6	1.97%	0.9951	0.015	0.99%	0.9986
SMO #7	2.15%	0.9948	0.016	1.20%	0.9982
SMO #8	2.44%	0.9921	0.016	1.27%	0.9976

two images. Most of the error comes from the dark spaces between the four quadrants of the polarizer. Close examination reveals another systematic effect. The center of each illumination spot appears somewhat dark, and there is a bright halo around each illumination spot. If the design image is convolved with a Gaussian "blurring" function, the quality of the fit can be greatly improved. Figure 4 shows the improvement after the design data is given a Gaussian blur with σ=1.1 pixels. After the blurring function is included, the RMS error of the data matching is reduced to 2.7% and the correlation increases to 0.9853. The image difference is now almost totally dominated by the dark spaces between the polarizer quadrants.

The color scale in figures 3 and 4 is expanded by a factor of 3 relative to the color scale for figures 1 and 2, in order to make the differences more visible.

The improvement in the quality of the fit when a Gaussian blurring function is added to the design data suggests that the pupil illumination is being widened by lens flare, defocus, or some similar optical effect. It is not know whether the spreading is induced by the Bertrand lens (in which case it is only a metrology artifact and will not show up in normal use), or if it is caused by manufacturing variability in the illumination aperture or optical scattering in the main imaging lens.

2.4 Summary of illuminator correlation to design

Table 1 shows the quality of the match to design for several illuminators. The RMS error and correlation value are shown for the measured image compared to the original illuminator design and also compared to the design convolved with a Gaussian blurring function. If the blurring of the illuminator image is an artifact of the Bertrand lens, then the second set of fitted numbers will be a better representation of the illuminator accuracy.

2.5 Discussion

The match of the pupil images to design is a worst-case evaluation, since some degradation by the Bertrand lens has been introduced into the measurement. The improved match of the pupil image to design when the Gaussian blurring function is included may be a best-case result, because some real image flare may be removed in addition to correcting for the effects of the Bertrand lens. Visually, the quality of the match to design is very good for all 14 cases evaluated, even without the added improvement of the Gaussian blurring function.

Although the accuracy of the physically rendered illumination is very good, there is a question of how much the residual errors in the illumination affect the image of a mask designed for use with such an illuminator. It is particularly important how residual illumination errors affect the evaluation of mask defects. In the next section, results are shown of image and defect evaluations, comparing simulated and measured aerial images with illumination sources of varying levels of accuracy.

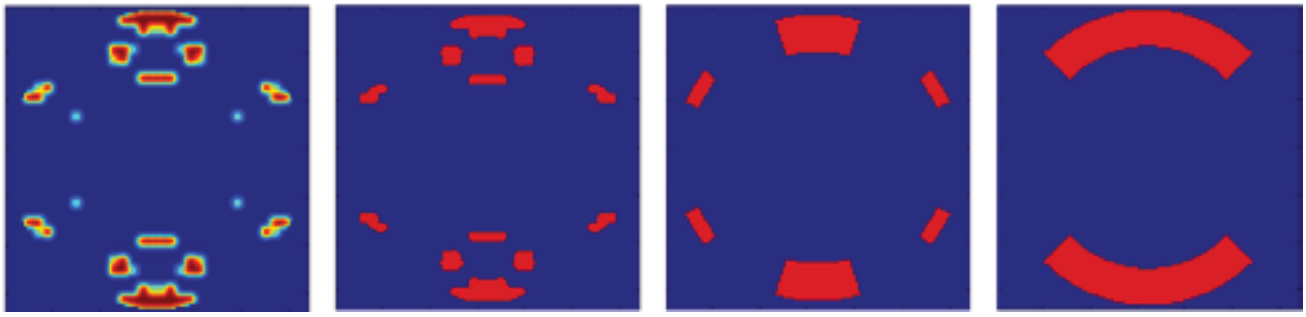

Figure 5. A series of approximations to a gray-scale SMO illuminator. From left to right, the original SMO illuminator design, a stencil design with the same contours, but no gray levels, a 6-pole design with approximately the same energy distribution, and a disar illuminator that poorly approximates the original illuminator design.

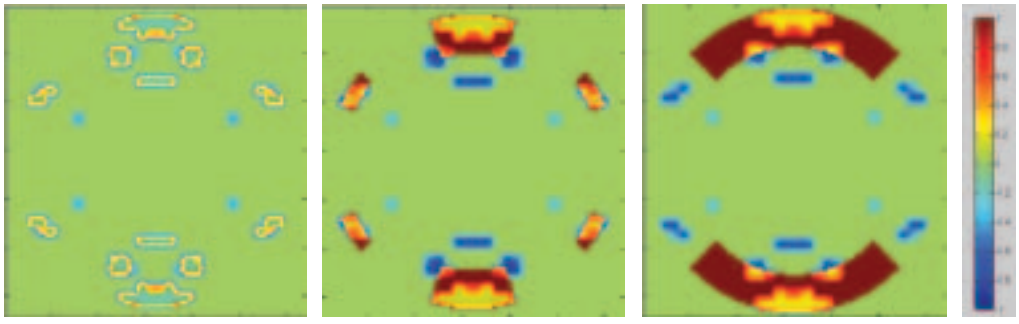

Figure 6. Difference between the approximate illuminator designs and the original gray-scale SMO illuminator.

3. Effects of Reduced Illumination Accuracy

To evaluate the effects of reduced illuminator accuracy, an SMO illumination pattern was selected and compared to a series of increasingly inaccurate approximations. Each of these approximate illuminators was used in the evaluation of a series of programmed defects on a photomask. The evaluations were done both in simulation and experimentally, on an AIMS™ system.

3.1 Experimental conditions

A mask with a series of programmed line-edge defects was built. A series of 25 defects was generated with the defect size varying from +36 nm to -36 nm in 2 nm increments. An SMO illuminator appropriate for the mask design was selected as the baseline illuminator for the experiment. This illuminator is the one labeled SMO#1 in Table 1 above. Three other illuminators, shown in figure 5, were selected to compare to this baseline case: a stencil illuminator with the same geometric pattern as the SMO illuminator, but without the gray-scale variations in intensity, a simple hexapole illuminator, and a disar illuminator.

Figure 6 shows the difference between the three approximate illuminator designs and the original gray-scale SMO illuminator, and table 2 lists the RMS error and correlation coefficient of the fit for each design.

Since these comparisons were done directly between illuminator designs, with no experimental measurement of the illumination profiles, the Gaussian blurring function was not applied to improve the quality of the fit.

Figure 7 shows the design of the programmed defect mask used for the evaluation.

Aerial image simulations were run using a commercial lithographic modeling program. The program used appropriate vector calculations for high numerical aperture immersion lithography, but did not include 3-dimensional electromagnetic field effects in the mask simulation. Figure 8 shows the ratio of aerial image size error to mask defect size, with both dimensions at mask scale. This value is the Mask Error Enhancement Factor (MEEF) of the defect for each type of illumination.

Not surprisingly, the MEEF of each approximation to the gray-scale SMO illumination design changes systematically as the illuminator accuracy deviates more and more from the original.

3.2 Experimental AIMS™ measurements

AIMS™ images of the same defect through a range of defect sizes were recorded for each of the illuminators in Figure 5.

The AIMS™ image was captured using a method which corrects for vector effects in aerial images at ultra-high numerical aperture. Sensitivity to the defect was derived from the AIMS™ images, and compared to the results of optical simulations using the same mask design and illuminator types.

The line width change in the AIMS™ aerial image was graphed against the size of the programmed mask defect (figure 9). The aerial image threshold was selected to make the width of the central line be equal to its design dimension when the defect size is zero. The 0.6219 slope of the graph represents the MEEF for this defect type using the gray-scale

Table 2. Quality of match to design for 3 different illuminator types. The second and third columns show RMS error and correlation coefficient for the illuminator design, compared to the original SMO illuminator.

Mask type and identification	RMS error of fit	Correlation coefficient
Stencil approximation	8.82%	0.9343
6-pole approximation	22.91%	0.5812
Disar approximation	37.09%	0.3187

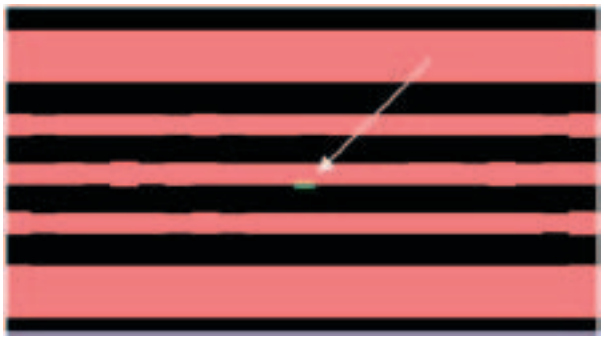

Figure 7. Design of programmed defect mask used for this study. The defect is indicated with an arrow.

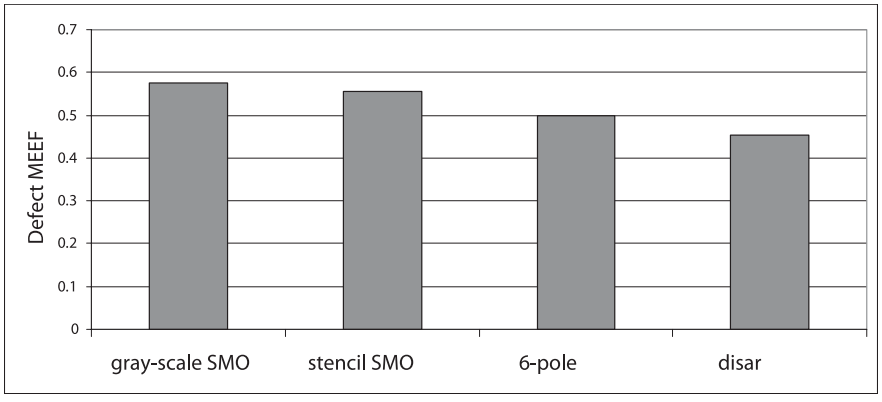

Figure 8. Mask Error Enhancement Factor for the sample mask defect under four different illumination conditions.

SMO illuminator design.

Different MEEF values were found, depending on which type of illuminator was used. The light bars in figure 10 show the experimentally measured change of sensitivity for the four illuminator types studied. The dark bars are the results of the simulations from figure 8.

Although the trend of the experimental data follows the simulation results, the experimentally measured defect sensitivity was systematically smaller than that of the computer simulations. Several investigations were made to understand the mismatch.

3.3 Discrepancies between simulation and data

The simulations used for this work had several known approximations: The mask shapes and illumination patterns were taken directly from design instead of from measured images, so imperfections of the illuminator and mask effects (such as corner rounding) were not captured. The simulations did not include a 3-dimensional model of the mask structure, which can have a significant effect. In addition, the simulation assumed aberration-free optics, and the effects of any aberrations in the lenses use for the data capture were unknown. Finally, there was concern about repeatability of the data. Some of the measurements were made over a period of several months, and the stability of the measurements was not known.

Long-term repeatability was checked by recapturing one set of images after an interval of seven months, and short-term repeatability was tested after an interval of twenty days. In all cases, the defect MEEF measurement repeated within ±1.5%.

The contribution of mask corner rounding was investigated by converting scanning electron microscope (SEM) images to a binary format that could be used as a direct input to the lithographic simulation program. Figure 11 shows the maximum clear defect and maximum opaque defect on the programmed defect mask, converted into the binary format.

Captured images of the AIMS™ pupil illumination were also used as inputs to the simulation program. This corrects for minor accuracy errors of the manufactured illumination aperture, but may introduce some artifacts from flare or defocus in the Bertand lens used to capture the image of the illumination.

It was found that using the digitized mask measurement in the simulations typically reduced the predicted defect MEEF by about 1%. Using the measured AIMS™ pupil illumination in the simulations increased the predicted defect MEEF by 2%. The two results combined linearly, so the net result of using digitized mask measurements and measured illumination maps in the same simulation increased the predicted defect MEEF by 1%.

In the next level of refinement, the simulations were run with a Finite Difference Time Domain (FDTD) modeling program that includes 3-dimensional mask effects and rigorous

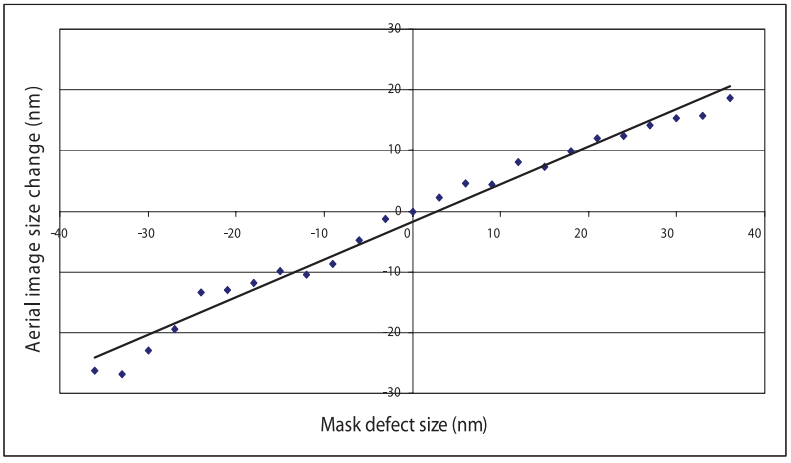

Figure 9. Size change of the measured aerial image vs size of the programmed mask defect, using the gray-scale SMO illuminator.

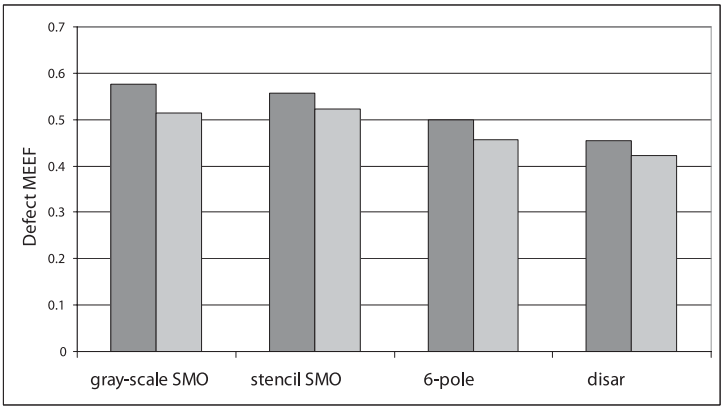

Figure 10. Experimentally measured defect MEEF for four illumination types (light bars), compared to computer simulations (dark bars)

EDITORIAL (continued from page 3)

As it is, the fortunes of the photomask industry are tied directly to the health of the semiconductor industry. Any forecast growth in semiconductors has the potential to be good news, because it invariably means new device designs in the pipeline. New and even revised device designs drive the photomask business, particularly when the semiconductor industry moves to new technology nodes as has happened over the past two years (45nm, 32nm & 22nm).

The volume trend for Photomasks remains flat, but as usual, the higher prices commanded by advanced masks should bring some revenue growth. Most major captive IDMs and several of the larger Foundry chip makers are already moving to 22nm device production raising the design volume and demand for advanced mask sets. Many of the associated optical lithography schemes now include double (and sometimes triple) patterning raising the number of critical (and more expensive) mask layers per set.

The looming question for advanced Photomask manufacturers is, "Are we really approaching the end of optical lithography?" There remains enormous uncertainty surrounding all the next generation lithography schemes (i.e. EUV, Imprint, DSA, etc.), none of which is a clear winner. New mask making capability will need to be developed for most of these technologies. But, where do we invest our limited capital in the near term to be ready for the product demands of the future? This has most mask makers rightly holding on to their capital budgets tighter than ever.

We've come through some difficult times recently and 2012 looks to be no less challenging. On the other hand, if the Mayans were right, the end of 2012 will be the end of this age of man, making all concerns over next generation lithography a moot point.

That's where we stand folks. Here's wishing you all a very happy holiday season and a profitable end to 2011. Hopefully, the most recent forecasts are correct and 2012 will continue to be a period of growth, and with a little luck, a time where the smoke begins to clear on the ultimate direction of NGL and the mask making technology needed to support it.

Figure 11. SEM contours of mask patterns for the maximum clear defect (left) and opaque defect (right).

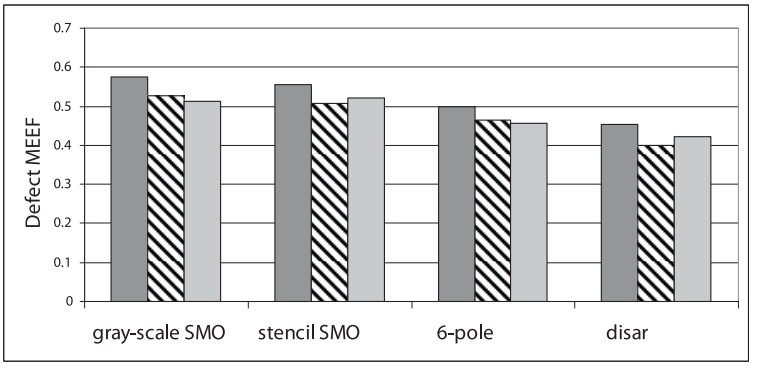

Figure 12. Experimentally measured defect MEEF for four illumination types (light bars), compared to computer simulations using a rigorous EMF model (striped). The non-EMF model results are shown for reference (dark bars).

electromagnetic field (EMF) calculations. The program used for this purpose could not easily accept the digitized mask measurements, so the original design shapes of the mask and illuminator were used as input. Inclusion of EMF effects predicted a defect MEEF much smaller than the thin-mask simulations, typically by 9%. As shown in figure 12, this gave improved agreement with the experimental AIMS™ data for all illumination types.

Finally, an attempt was made to include measured lens aberrations in the simulations. The first simulations run with aberrations in the optical model showed unexpectedly large effects, but these effects were not repeated when running a different simulation program. Because of this discrepancy, the results of simulations with lens aberrations are not reported here, and work is continuing to understand the effects of aberrations.

4. Conclusions

Manufactured gray-scale illumination apertures for AIMS™ have been evaluated against the original illuminator designs and found to be very accurate, typically within 1.8-3.4% RMS of the design. Correction for image blurring in the data collection optics brings the agreement to a range of 1.0- 2.7% RMS. insensitive to illuminator errors much larger than the manufacturing errors measured in this study. Experimental data from AIMS™ showed a trend similar to the simulations, but with somewhat lower sensitivity to the defects. Much of the discrepancy was explained by adding additional levels of improvement to the simulations, especially by the inclusion of EMF effects.

5. References

[1] Russell A. Budd, Derek B. Dove, John L. Staples, H. Nasse, and Wilhelm Ulrich, “A new mask evaluation tool, the microlithography simulation microscope aerial image measurement system”, **Proc. SPIE 2197,** 530-540 (1994).

[2] W. Harnish, “Microlithography simulation microscope: mask evaluation under stepper conditions”, Mask Technology for Integrated Circuits and Micro-Components GMM-Fachbericht, Vol. 23, 43-52 (1996).

[3] Alan E. Rosenbluth, Scott J. Bukofsky, Michael S. Hibbs, Kafai Lai, Antoinette F. Molless, Rama N. Singh, and Alfred K. K. Wong, “Optimum mask and source patterns to print a given shape”, **Proc. SPIE 4346,** 486 (2001).

[4] Alan E. Rosenbluth, David O. Melville, Kehan Tian, Saeed Bagheri, Jaione Tirapu-Azpiroz, Kafai Lai, Andreas Waechter, Tadanobu Inoue, Laszlo Ladanyi, Francisco Barahona, Katya Scheinberg, Masaharu Sakamoto, Hidemasa Muta, Emily Gallagher, Tom Faure, Michael Hibbs, Alexander Tritchkov, and Yuri Granik, “Intensive optimization of masks and sources for 22nm lithography”, **Proc. SPIE 7274,** 727409 (2009).

Industry Briefs

Highlights from EUV Symposium

By **Stefan Wurm**, SEMATECH's lithography, ElectroIQ

AIMS
Zeiss reported on the repair strategies for EUV with an aerial image measurement system (AIMS) for actinic inspection of reticle defects and on the EUV Mask Infrastructure (EMI). Defect size/density are about in step with the industry's current improvement rate, but defect localization and pattern shifting is a potential game-changer. SEMATECH is "seriously exploring" improving productivity for the AIMS and other actinic inspection tools by enabling a high-brightness source.

Defects
GlobalFoundries, IBM, Intel, Toshiba, and TSMC showed progress in developing defect avoidance and mitigation to use masks with a few remaining defects. Current mask defect levels are expected to support DRAM for pilot line operation soon while lower mask defect levels are required to meet logic/foundry requirements. Amplitude defects are less frequent than phase defects but are present on every mask. Industry roadmap for amplitude defects is called for. SMT modeling and programmed amplitude-defect mask development has begun. Preliminary substrate-defect roadmapping appears to be overly conservative, though sensitivity requirements are likely below current inspection tool's capabilities. Missed substrate defects can be picked up at ML blank inspection, but cost/cycle time impact might be acceptable. ML blank defect density today: 29 EUV mask blanks (Lasertec M7360) shows 2911 pits (~100/mask) and 484 particles (~17/mask). Cumulative blank yield, without localization and pattern shifting, shows 10% yield at >45nm sensitivity; 50% at 72nm; and 75% for 175nm threshold. Issues cropping up at <16nm nodes include: interference stack parameters, aperture, pupil fills, CRA, and defect types.

Resists
Several chemically amplified resist (CAR) materials achieving sub-20nm resolutions were demonstrated including a 15nm half-pitch resolving CAR and a nanoparticle resist demonstrating mid-20nm half-pitch resolution at excellent photosensitivity.

Priorities
Samsung assessed the pilot-line readiness of EUV, and outlined the timetable and performance requirements for high-volume manufacturing for DRAM (in 2013).

The EUVL Symposium Steering Committee identified three remaining focus areas that the industry needs to work on to enable EUVL manufacturing insertion: 1) Long-term reliable source operation, 200W at IF, 2) Mask yield & defect inspection/review infrastructure; 3) Resist resolution, sensitivity, and LER met simultaneously.

Next-gen litho not named EUV
Simultaneous with the EUV Symposium was the Lithography Extensions Symposium, focusing on other patterning techniques to extend resolution capabilities more cost-effectively than EUV. Directed self-assembly (DSA) is making significant progress toward potential commercial application in IC manufacturing. A variety of techniques including chemo-epitaxy, graphoepitaxy, and spin-on spacer, were all demonstrated as potential DSA based patterning approaches. Resist and chemical suppliers (e.g., AZ, JSR, DOW) have development activities underway. IBM reported improvement in the patterning capability of existing lithography systems through contact hole rectification. Progress was made toward development of a mesoscale model to help predict material interactions to identify materials for DSA applications. SEMATECH's Nanoimprint demonstrated overlay capability of 15nm and defectivity of <0.1>2 showing potential for achieving defect levels commensurate with manufacturing requirements.

Join the premier professional organization for mask makers and mask users!

About the BACUS Group

Founded in 1980 by a group of chrome blank users wanting a single voice to interact with suppliers, BACUS has grown to become the largest and most widely known forum for the exchange of technical information of interest to photomask and reticle makers. BACUS joined SPIE in January of 1991 to expand the exchange of information with mask makers around the world.

The group sponsors an informative monthly meeting and newsletter, BACUS News. The BACUS annual Photomask Technology Symposium covers photomask technology, photomask processes, lithography, materials and resists, phase shift masks, inspection and repair, metrology, and quality and manufacturing management.

Individual Membership Benefits include:

- Subscription to BACUS News (monthly)
- Complimentary Subscription *Semiconductor International* magazine
- Eligibility to hold office on BACUS Steering Committee

spie.org/bacushome

Corporate Membership Benefits include:

- Three Voting Members in the SPIE General Membership
- Subscription to BACUS News (monthly)
- One online SPIE Journal Subscription
- Listed as a Corporate Member in the BACUS Monthly Newsletter

spie.org/bacushome

Calendar

2012

Advanced Lithography

12-16 February 2012
San Jose Convention Center and San Jose Marriott
San Jose, California, USA
spie.org/alcall

SPIE Photomask Technology

10-13 September 2012
Monterey Marriott and Monterey Conference Center
Monterey, California, USA
spie.org/pm

You are invited to submit events of interest for this calendar. Please send to lindad@spie.org; alternatively, email or fax to SPIE.

SPIE is an international society advancing light-based technologies.

SPIE

International Headquarters
P.O. Box 10, Bellingham, WA 98227-0010 USA
Tel: +1 360 676 3290
Fax: +1 360 647 1445
help@spie.org • SPIE.org

Shipping Address
1000 20th St., Bellingham, WA 98225-6705 USA

SPIE Europe

2 Alexandra Gate, Ffordd Pengam, Cardiff,
CF24 2SA, UK
Tel: +44 29 2089 4747
Fax: +44 29 2089 4750
spieeurope@spieeurope.org • www.spieeurope.org